American Mineralogist, Volume 81, pages 1166–1175, 1996

Stratigraphy of the lunar highland crust: Depths of burial of lunar samples from cooling-rate studies

I.S. McCallum and Hugh E. O'Brien

Department of Geological Sciences, University of Washington, Seattle, Washington 98195, U.S.A.

Abstract

Current models of lunar crustal stratigraphy are based primarily on models of impact cratering coupled with what is known about the distribution of rock types in the ejecta blankets associated with the large multiring basins. These models postulate an upper crust rich in the ferroan anorthosite component underlain by a more mafic (noritic) lower crust (Spudis 1993). We attempted to test these models by determining the depth at which various lunar plutonic rocks formed. Despite intense brecciation and shock, many lunar highland samples retain vestiges of a prior magmatic history. For example, pyroxene samples preserve a record of their thermal history in such phenomena as cation ordering and exsolution textures. By computer simulation of the growth of exsolution lamellae in augite and pigeonite, we deduced cooling rates and from these estimated a depth of burial on the basis of a simple model for the thermal evolution of the lunar crust. Despite the fairly large uncertainties in the calculations, it is clear that the ferroan anorthosite samples we studied formed at a depth between 10 and 20 km, whereas some members of highland magnesian and alkali suites formed as cumulates in magma chambers intruded into the uppermost layers of the crust. As yet there is no evidence to indicate that crystalline rocks from the lower half of the lunar crust are present in the samples returned by the Apollo missions. Most samples derived from the lower crust appear to be impact melts of low-K Fra Mauro (noritic) composition.

Introduction

One of the most difficult, yet important, problems facing lunar geologists is that of reconstructing the stratigraphy of the lunar crust and its evolution over time. Intense bombardment and mixing of rock types during the first 600 m.y. of lunar history has rendered this task especially difficult. At the same time, impact processes have brought to the lunar surface samples derived from at least the upper half of the lunar crust, thereby providing an opportunity to reconstruct the stratigraphy in areas sampled during the Apollo missions. As noted by Spudis (1993) in his review of the geology of multiringed basins, there is general agreement that ejecta from the large multiring basins are dominantly, or perhaps even exclusively, of crustal origin since 25 yr of lunar sample study have failed to identify any unequivocal mantle samples. Given the most recent determination of crustal thickness (Zuber et al. 1995) this implies an upper limit to the depth of excavation of around 60 km. Magma-ocean models (Warren 1990) postulate an upper crust dominated by anorthositic rocks that formed by flotation in the primordial magma ocean; but on nearside areas sampled by Apollo missions, anorthosite is common only at the Apollo 16 site in the central highlands and rare to absent at all other landing sites. A preliminary analysis of the Clementine multispectral data has revealed that anorthosite is not widely exposed on the lunar nearside and is most commonly observed in inner basin rings of the southern highlands, e.g., the massifs of the Inner Rook Mountains of the Orientale basin, and isolated occurrences such as the central peak of Aristarchus crater (Hawke et al. 1995). However, the Clementine data suggest that anorthosite may be quite abundant on farside regions.

Basin impact melts, most notably the low-K Fra Mauro composition associated with the Imbrium and Serenitatis basins, are distinctly more mafic, with a composition corresponding to norite. Cratering models suggest that such melts are generated at lower to middle crustal depths (30–60 km). The paucity of unequivocal deep-seated crystalline plutonic rocks is also consistent with cratering models that suggest that unmelted rock fragments in ejecta blankets are probably derived from the upper part of the crust (Spudis 1993). Consequently, the possibility exists that no crystalline lunar samples from deeper that about 30 km are present in the collection of samples returned.

Lunar highland plutonic rocks belong to at least two separate chemical groups, the ferroan anorthosite suite (FAS) and the Mg-rich suite (James 1980; Norman and Ryder 1980). Although there is general agreement that ferroan anorthosites form a coherent group and probably

0003–004X/96/0910–1166$05.00

share a common origin by flotation accumulation in a global magma ocean, the Mg suite, on the other hand, is more compositionally diverse and comprises two main groups: a highland magnesian suite (HMS) composed of dunite, troctolite, norite, and gabbronorite, and a highland alkali suite (HAS) composed of anorthosite, gabbronorite, quartz monzodiorite, and granite (felsite). A petrogenetic link between these two series has not been firmly established, although such a link has been suggested (Snyder and Taylor 1995) because many HMS and HAS samples share important geochemical characteristics, e.g., low Ti/Sm and Sc/Sm ratios and enrichment in incompatible elements relative to ferroan anorthosite (Norman and Ryder 1980). Currently favored models suggest that HMS and HAS plutonic rocks crystallized from KREEP-contaminated endogenic magmas emplaced in the crust after the anorthositic crust formed but before the major basin-forming impacts. Geochronologic evidence is somewhat ambiguous on this point because ferroan anorthosite and Mg-suite samples show some overlap of ages (Carlson and Lugmair 1988; Nyquist et al. 1981; Premo and Tatsumoto 1992, 1993; Shih et al. 1993), although Mg-suite samples are, on average, slightly younger with more evolved initial isotopic ratios. Within the magnesian and alkali suites there are subsets of samples, e.g., gabbronorite, that show distinct geochemical differences, lending credence to the suggestion that a variety of magma types was generated by internal melting processes early in lunar history. The isotopic evidence is also difficult to reconcile with a single magma type (Shih et al. 1993). Finally, although the evidence from the Apollo 15 and 17 impact-melt sheets is consistent with a noritic lower crust, it is not known whether some of the Apollo 17 cumulate norite samples are from this crustal layer or are fragments derived from a high-level intrusion.

One parameter that could provide an important piece to the puzzle, but which has proven very difficult to quantify, is the depth at which lunar crustal rocks crystallized or, in some cases, recrystallized. This task is particularly difficult because highland samples have been severely degraded (at least texturally), many have been recrystallized at high temperature, and most have been subjected to some reheating in ejecta blankets. Computations of depths of equilibration using experimentally calibrated geobarometers are of limited value on the Moon because of the low pressure gradients (~0.05 kbar/km) and the lack of phases sensitive to low pressure variations. The most promising approach appears to be the independent determination of the cooling rate of a plutonic sample because cooling rates can be used to calculate a depth of burial assuming that thermal conductivities and an appropriate crustal cooling model are available. In this work we describe a method to determine cooling rates by measuring the width, spacing, crystallographic orientation, structural state, and composition of exsolution lamellae in pyroxene and from these cooling rates to infer burial depths.

Method

Profile measurement

Major and minor elements in pyroxene were analyzed using a JEOL 733 Superprobe equipped with four wavelength-dispersive spectrometers. All analyses were performed using an accelerating voltage of 15 kV. ZAF corrections were applied to all microprobe analyses. Compositional profiles were measured across host–(001) lamellar pairs in augite and pigeonite from a variety of lunar highland samples. Most of the pigeonite grains have inverted to orthopyroxene. Grains in which the (001) lamellae are oriented perpendicular to the surface of the section were selected on the basis of optical properties, and, insofar as it was possible, profiles were measured parallel to the c axis. For pyroxene with lamellar widths ≥ 5 μm, a programmed step interval of 1 μm was used, and up to several hundred points per grain were analyzed for Ca, Mg, Fe, Al, Ti, Cr, and Na. For pyroxene with lamellar widths <5 μm, step scanning at 1 μm intervals proved inadequate to determine the details of compositional variations because in many cases, the diameter of the excitation volume was larger than the lamella being analyzed. To address the problem of lack of resolution we adopted a beam-scanning technique in which an area encompassing several host–lamella pairs was scanned and X-ray counts corresponding to Ca, Mg, Fe, and Al were collected during scanning. The pixel size varied depending on the area scanned, e.g., an area of 20 × 20 mm has pixels of 0.045 mm. Counting times of up to 24 h were required to obtain a statistically meaningful number of counts per pixel. Counts were converted to weight percent using correction factors obtained from conventional probe analysis. This method does not, of course, improve resolution, but it does provide a much larger data set, which greatly improves deconvolution calculations. Application of this method to the narrow lamellae in pyroxene from quartz monzodiorite is discussed later in this paper.

In addition to the standard correction procedures, it is essential to correct the data for overlap effects in the vicinity of lamella–host interfaces because the measured composition represents a weighted average of the volume of sample excited by the electron beam (Ganguly et al. 1988). The magnitude of the overlap effect is different for different elements and is primarily a function of the excitation voltage. The volume of excitation around the incident beam is assumed to have a radially symmetric Gaussian intensity distribution with a standard deviation (ϵ), which can be calculated from the slope of the measured profile at the interface. For Ca, ϵ has a value of 0.55. Because deconvolution is extremely difficult to perform, we followed the method of Ganguly et al. (1988), in which a hypothetical concentration profile is convolved and this profile is then adjusted until the calculated, convolved profile agrees with the measured profile within the analytical uncertainty. In practice, it is usually necessary to correct the raw data for a distance of only a few micrometers on either side of the interface. However,

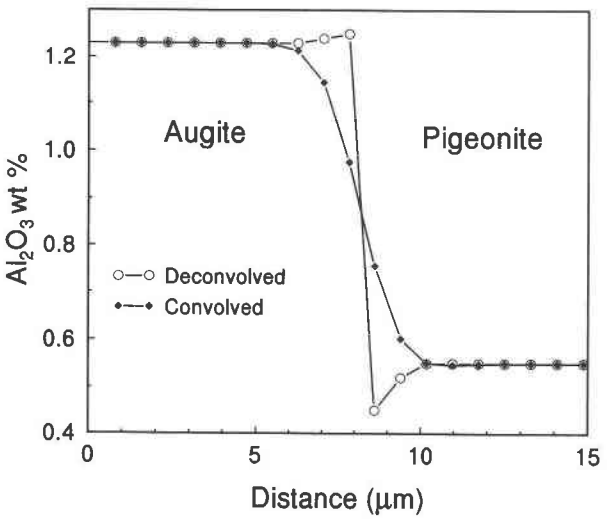

FIGURE 1. Example of deconvolution techniques used to correct for effects of spatial averaging on microprobe traverses across host-lamella boundaries. Value of ϵ is 1.0.

as shown in Figure 1, in which convolved and deconvolved profile for Al_2O_3 are compared, the effect of the spatial averaging can be significant.

Closure temperatures

It is important to have knowledge of the temperature range over which interdiffusion of Ca and Fe/Mg on the micrometer scale is effective. An estimate of the closure temperature is made from the composition of host and lamellar pairs. The compositions are plotted on the Sack and Ghiorso (1994) phase diagram, which shows the 1100 and 800 °C isotherms on the pyroxene solvus as a function of composition (Fig. 2). Because most of the data plot at, or slightly below, the 800 °C isotherm, it was assumed that diffusion on the micrometer scale resolvable by microprobe analysis was ineffective below approximately 800 °C.

Solution of diffusion equation

Because the (001) lamellae in augite and pigeonite grow along a planar front by interdiffusion of Ca and MgFe parallel to the c axis, a one-dimensional solution to the diffusion equation is sufficient. To simulate lamellar growth, we modified a computer program (Sanford 1982) that provides a numerical solution to the diffusion equation and allows for compositional and temperature-dependent diffusion coefficients. A summary of the appropriate equations and computational method is given in Miyamoto and Takeda (1994). Diffusion coefficients of Ca (D_{Ca}) parallel to c in augite and pigeonite were determined by Fujino et al. (1990, and 1993 personal communication) at 50 °C intervals from 1200 to 1000 °C. These values are as follows: For $T > 1100$ °C, $D_{Ca(Aug)} = 1.43 \times 10^{-1}$ cm²/s exp $(-100.2$ kcal/R$T)$ and $D_{Ca(Pig)} = 1.28 \times 10^{2}$ cm²/s exp $(-110.2$ kcal/R$T)$; for $T < 1100$ °C, $D_{Ca(Aug)} = 3.81 \times 10^{-14}$ cm²/s exp $(-21.3$ kcal/R$T)$ and $D_{Ca(Pig)} = 5.88 \times 10^{-12}$ cm²/s exp $(-26.5$ kcal/R$T)$. These data agree reasonably well with the results of Brady and McCallister (1983), who obtained an average value of $D_{Ca(Aug)} = 3.89 \times 10^{-3}$ cm²/s exp $(-86.25$ kcal/R$T)$ for temperatures between 1100 and 1200 °C. The diffusion coefficients represent the major source of uncertainty in the computation of absolute cooling rates because a significant fraction of lamellar growth occurs at temperatures below 1000 °C. We used a linear extrapolation on a log D vs. $1/T$ plot to estimate diffusion coefficients below 1000 °C. There is also reason to believe that interdiffusion of Ca and FeMg in pyroxene is compositionally dependent (Ganguly and Tazzoli 1994).

An accurate representation of the pyroxene solvus is required. We used the solvus parameters recently determined by Sack and Ghiorso (1994). A projection of the 1100 and 800 °C isotherms on the 1 bar solvus is shown in Figure 2, and it is worth noting that this solvus is significantly different from earlier published versions (Lindsley 1983), which do not incorporate the effects of Fe-Mg ordering in the solution models. For the particular

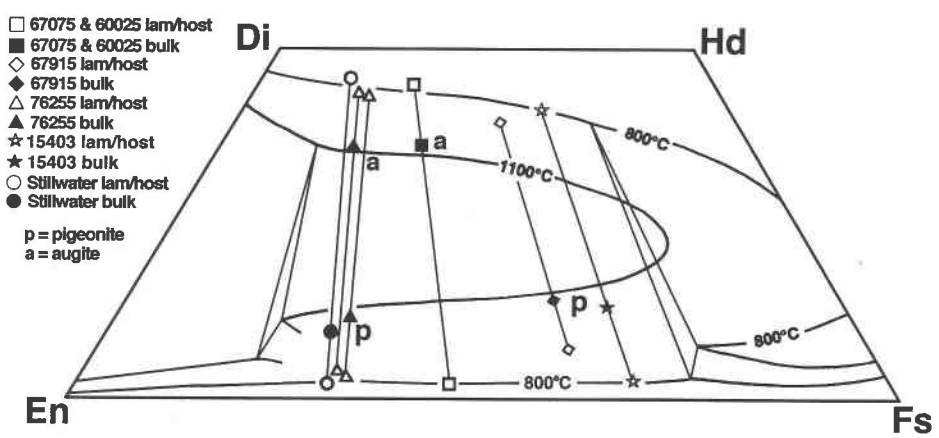

FIGURE 2. Compositions of pyroxene in terms of quadrilateral components. The 800 and 1100 °C solvus isotherms are from Sack and Ghiorso (1994). Solid symbols refer to bulk compositions, and open symbols refer to host and lamellar compositions.

composition being modeled, a section through the solvus at the appropriate Mg/(Mg + Fe) value was computed. Use of the correct solvus and tie lines in the model is critical because these determine the temperature of initiation of exsolution, the extent of exsolution, and the compositions of the host and lamellae as a function of temperature.

In the simulation of compositional profiles, it is necessary to specify an appropriate field length for diffusion. In practice, this is taken as one-half of the width of a lamella plus one-half of the width of an adjacent host as measured on the crystal for which a profile is being simulated. Critical input parameters are bulk Ca/(Ca + Mg + Fe) and Mg/(Mg + Fe) of the pyroxene. In coarsely exsolved pyroxene, these parameters were calculated by integrating the host and lamellar compositions in the appropriate proportions determined by image analysis of a backscattered electron (BSE) image of the grain. Linear and exponential cooling rate functions resulted in very little difference in the computed profiles.

Results

In this section we present the results of the modeling of compositional profiles of pigeonite and augite from two ferroan anorthosite samples (60025, 67075), a magnesian suite gabbronorite (76255), an alkali suite sodic ferrogabbro (67915), a quartz monzodiorite (15403), and an inverted pigeonite from a Stillwater gabbronorite (161). The main criterion in the selection of samples was the presence of optically visible exsolution lamellae in pyroxene. This limited our selection to samples containing coexisting low-Ca and high-Ca pyroxene because, as expected, samples containing a single pyroxene seldom contained well-developed exsolution features. The relevant compositional data are listed in Table 1.

Table 1. Host-lamella compositions and widths determined from microprobe profiles

Sample	Bulk Wo	Bulk En	Lam. Wo	Lam. En	Host Wo	Host En	Lam. width (μm)	Working half-width (μm)
67075,52 Aug	34.5	40.2	1.6	50.9	43.7	37.1	19	41
60025,130 Aug	35.2	40.8	1.9	51.8	43.6	37.0	37	85
76255,69 Aug	36.0	48.0	4.4	65.6	44.0	43.0	4.5	12.6
76255,70 Pig	10.0	62.6	42.8	43.3	2.8	65.6	21	60
67915,190 Pig	14.0	35.4	40.0	28.9	7.8	35.8	4.4	12
15403,71 Pig	13.3	30.0	41.5	24.8	2.3	32.3	2	3.2
SWC 161 Pig	9.4	63.1	46.2	41.8	2.0	67.3	17	46

Note: Lam. = lamella.

Ferroan anorthosite

Sample 67075 is a cataclastic ferroan anorthosite previously described by McCallum et al. (1975). Plagioclase (An_{97-98}) occurs as angular matrix grains and as recrystallized microanorthosite clasts, whereas pyroxene, which occurs as sparse grains, shows exceptionally well-developed exsolution lamellae (Fig. 3a). The low-Ca pyroxene grains in 67075 are inverted pigeonite with coarse augite exsolution, whereas augite grains show complex exsolution with several generations of pigeonite on (001) and (100). After exsolution as pigeonite from the augite host, the coarse (001) lamellae, which are up to 30 μm in width, have largely inverted to orthopyroxene. The coarse lamellae are comparable in width and composition (wollastonite content) to magmatic pyroxene in the Stillwater Complex and almost certainly were formed during the initial cooling from magmatic temperatures. The second-generation (001) pigeonite, which forms fine lamellae in sample 67075, is not observed in Stillwater augite, suggesting that the lunar pyroxene suffered a more complex thermal history possibly because of reheating and cooling in an ejecta blanket. Figure 4 shows a compositional profile (uncorrected for the overlap effect) across an augite (bulk composition of $Wo_{34.5}En_{40.2}Fs_{25.3}$) containing 20 μm wide (001) lamellae of low-Ca pyroxene. There are no resolvable compositional gradients in Ca, Fe, or Mg at the lamellar boundaries, but there are measurable gradients in Al and to a lesser extent Ti.

The "spikes" on the deconvolved Ca/(Ca + Mg + Fe) profile (Fig. 5) result from the beam impinging on the narrow, and incompletely resolvable, second-generation (001) lamellae. These compositional excursions were ignored in the modeling. Analyses on either side of the interface were corrected for the beam-overlap effect. The deconvolution factor is very sensitive to location of the analytical spot relative to the interface, and a change in position of as little as 0.1 μm can have a significant effect. Depending on the choice of interface position, the measured profile may be undercorrected in some cases and overcorrected in others. The calculated profile, obtained using the parameters listed in Table 1, represents the best fit to the measured profile. The calculated cooling rate of 3.7×10^{-5} °C/yr must be considered as an upper limit for this augite because it had exsolved the maximum amount of (001) pigeonite possible at its closure temperature, as indicated by the absence of any gradient in Ca, Mg, or Fe within the resolution of the microprobe. In cases in which the profiles are effectively step functions, the resolution required to calculate a unique cooling rate is lost. Additional information, e.g., diffusion rates of the more slowly diffusing cations Al and Ti, is required to refine the cooling rate.

Sample 60025 is also a cataclastic ferroan anorthosite with abundant An_{97-98} plagioclase and sparse, exsolved augite grains (Ryder 1982). There are large modal variations in sample 60025, depending on which subsample is being studied; subsamples studied by James et al. (1991) have significantly more low-Ca pyroxene than augite. There is an absence of compositional gradients in all elements analyzed. The bulk composition of the grain we analyzed is difficult to compute because the grain represents only a fragment of a larger grain. We used a bulk composition of $Wo_{35.2}En_{40.8}Fs_{24.0}$. The fine structure in this pyroxene is similar to that in the grain in sample 67075,52 described above. The calculated profile superimposed on

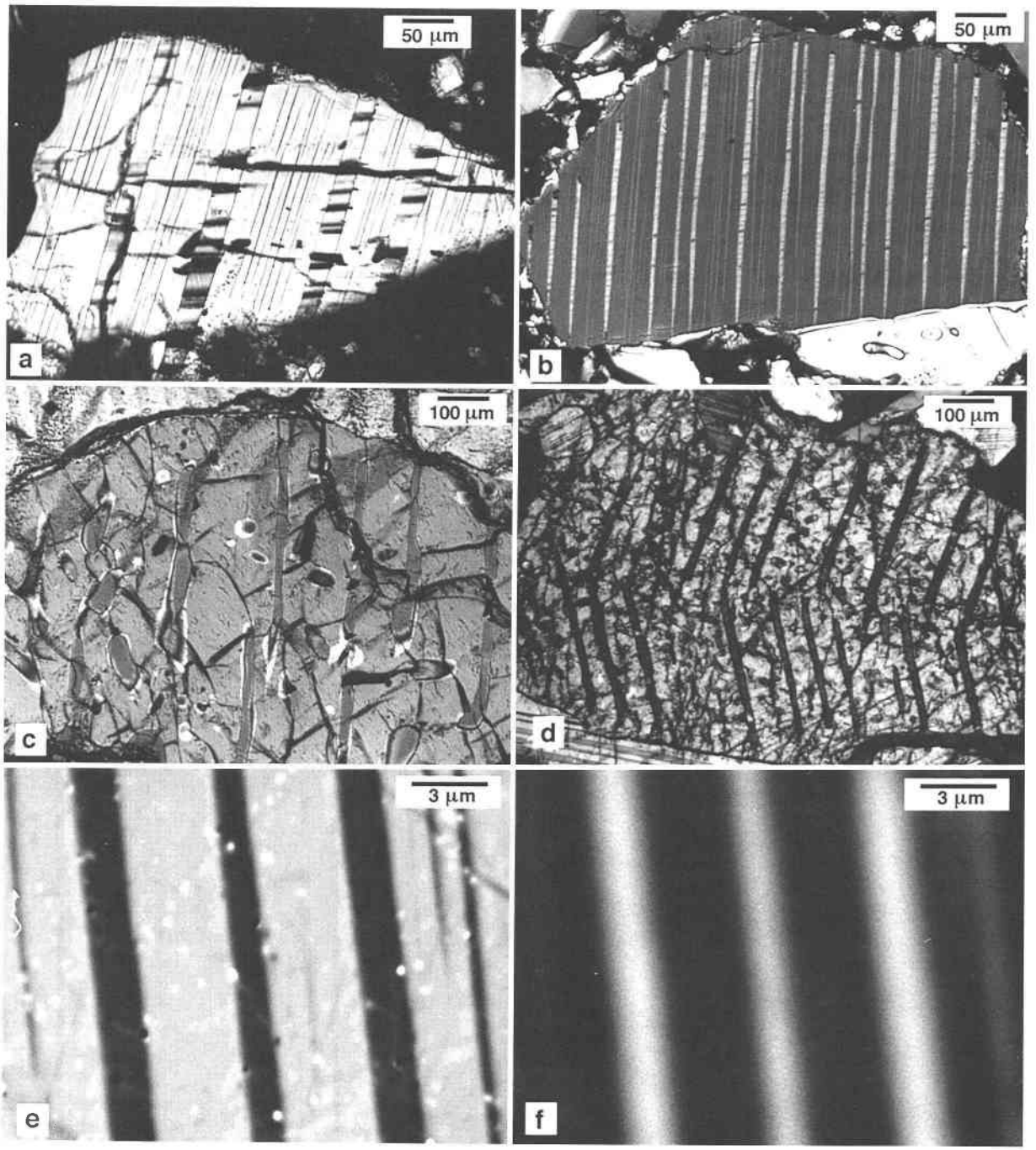

FIGURE 3. Images of lunar pyroxene. (**a**) Augite from ferroan anorthosite 67075,52, showing several generations of exsolution features. The wide lamellae are (001) pigeonite inverted to orthopyroxene, whereas the fine (001) lamellae are not inverted. (**b**) Augite from gabbronorite 76255,70, showing two generations of (001) lamellae. The thickest lamellae are ~5 μm wide. (**c**) The (001) lamellae of augite (10–25 μm) in inverted pigeonite from 76255,69. Note the blebby exsolution and the similarity to Stillwater inverted pigeonite shown in **d**. (**d**) Inverted pigeonite from gabbronorite 161 (Stillwater Complex) containing relict (001) lamellae of augite. The herringbone pattern indicates a (100) twin plane in the original pigeonite prior to inversion. Note also the blebby exsolution typical of many pigeonite samples. (**e**) Backscattered electron (BSE) image of an exsolved ferropigeonite from 15403,71. (**f**) Ca$K\alpha$ X-ray map of the same area of the ferropigeonite grain shown in **e**. Note the much higher resolution of the BSE image in comparison with the X-ray image.

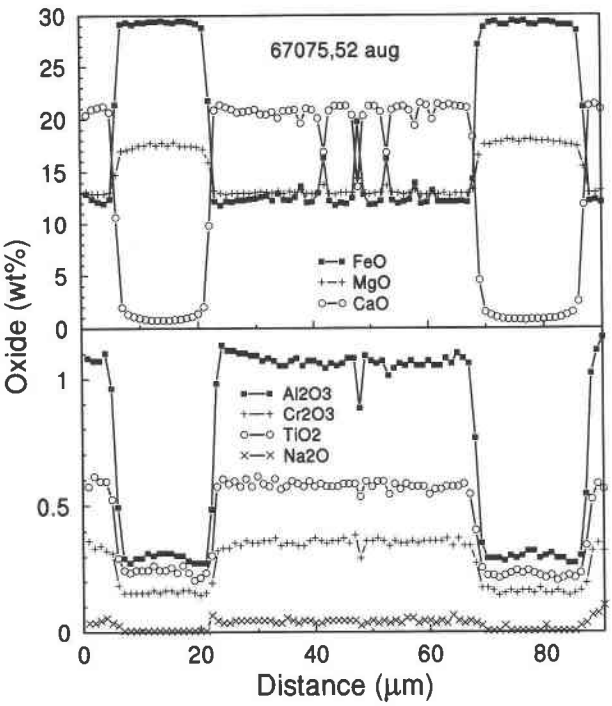

FIGURE 4. Compositional profile across host and lamellae in augite from 67075,52. Spikes in the profile are due to incompletely resolved second-generation exsolution lamellae. Note the slight compositional gradients in Al_2O_3 and TiO_2.

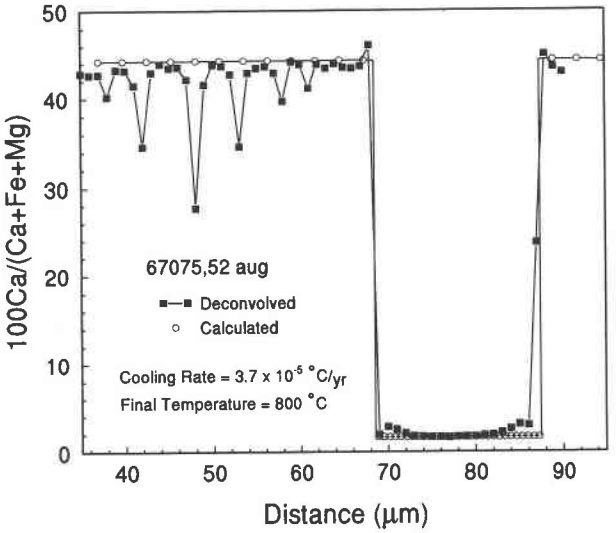

FIGURE 5. Measured (deconvolved) and calculated profiles in a traverse across a pigeonite lamella and augite host in anorthosite 67075,52. Deconvolution factor $\epsilon = 0.55$. Second-generation lamellae were ignored in the modeling.

the deconvolved profile indicates an upper limit cooling rate of 1.8×10^{-5} °C/yr (Fig. 6).

Magnesian suite

Samples 76255,69 and 76255,70 are thin sections of gabbronorite clasts from the polymict impact-melt breccia collected from the Station 6 boulder (Simonds et al. 1974). Both sections contain exquisite examples of complexly exsolved augite and inverted pigeonite (Figs. 3b and 3c). The (001) pigeonite lamellae in augite show no evidence of inversion. The (001) augite lamellae in the inverted pigeonite are up to 20 μm in width, whereas the corresponding (001) pigeonite lamellae in augite are typically around 5 μm in width. This is consistent with the larger Ca diffusion coefficients for pigeonite. Compositional gradients, particularly for Al and Ti, at the lamellar boundaries in both augite and pigeonite are much more pronounced than those in the FAS pyroxene. Compositional gradients for Ca, Fe, and Mg became apparent after the profiles were deconvolved (Fig. 7). The bulk composition of the augite grain that we modeled is $Wo_{36}En_{48}Fs_{16}$ (Fig. 2), and the calculated cooling rate is 3.2×10^{-2} °C/yr, i.e., nearly three orders of magnitude faster than that calculated for the FAS samples.

The deconvolved profile of 76255,69 pigeonite ($Wo_{10.0}En_{62.6}Fs_{27.4}$) also shows large compositional gradients at the lamellar boundary, particularly in Al, Ti, and, to a lesser extent, Ca (Fig. 8). The best-fit computed profile gives a cooling rate of 3.3×10^{-2} °C/yr, essentially the same as that determined for the coexisting augite described above.

Sodic ferrogabbro

Samples 67915,190 and 191 are thin sections from a sodic ferrogabbro clast in a polymict breccia collected from Outhouse Rock. This clast probably belongs to the highland alkali suite. The section consists of relatively Na-rich plagioclase (An_{54-69}), ferroaugite, ferropigeonite, a silica mineral, ilmenite, and trace amounts of apatite, whitlockite, troilite, iron metal, and baddelyite (James

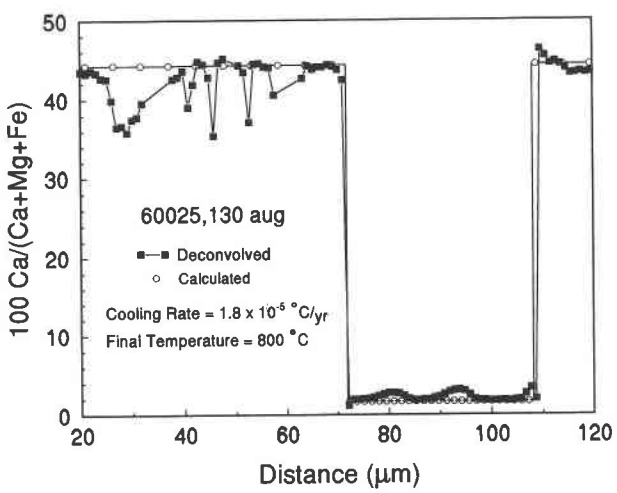

FIGURE 6. Measured (deconvolved) and calculated profiles in a traverse across a pigeonite lamella and augite host in anorthosite 60025,130. Value of ϵ is 0.55. Second-generation lamellae were ignored in the modeling.

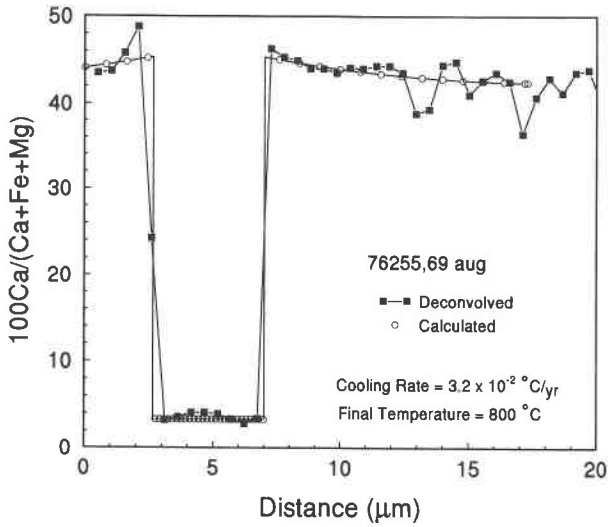

FIGURE 7. Measured (deconvolved) and calculated profiles in a traverse across augite host and pigeonite lamella from gabbronorite 76255,69. Value of ϵ is 0.55.

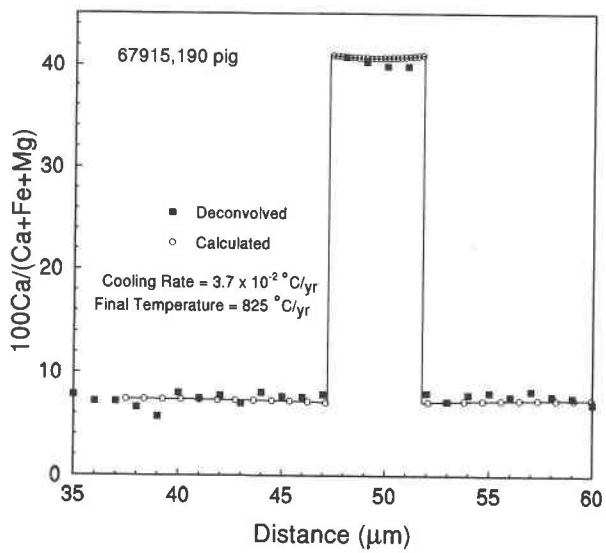

FIGURE 9. Measured (deconvolved) and calculated profiles in a traverse across pigeonite host and augite lamella from sodic ferrogabbro 67915,190. Value of ϵ is 0.55.

and Flohr 1983; McCallum and O'Brien, unpublished data). Coexisting ferroaugite and ferropigeonite in 67915,190 and 191 have well-developed exsolution lamellae approximately 3 and 5 μm wide, respectively. The bulk composition of ferropigeonite as determined by image analysis ($Wo_{14.0}En_{35.4}Fs_{50.6}$) is identical to that determined by Taylor et al. (1979) using wide-beam microprobe techniques. Even though the augite lamellae in this ferropigeonite are significantly narrower than those in 76255, the calculated cooling rate of 3.7 × 10^{-2} °C/yr (Fig. 9) is only slightly larger, reinforcing the point that the magnitudes of diffusion-generated compositional gradients are more accurate indicators of cooling rate than are lamellar widths.

Quartz monzodiorite

The quartz monzodiorite examined in this work occurs as a clast in thin section 15403,71. This clast is unusually rich in apatite and whitlockite and contains plagioclase, pyroxene, and oriented granophyric intergrowths of silica and potassium feldspar (Marvin et al. 1991). The pyroxene is unzoned, Fe-rich (Fig. 3), and shows finely exsolved lamellae of ferroaugite in ferropigeonite. A Ca$K\alpha$ map for

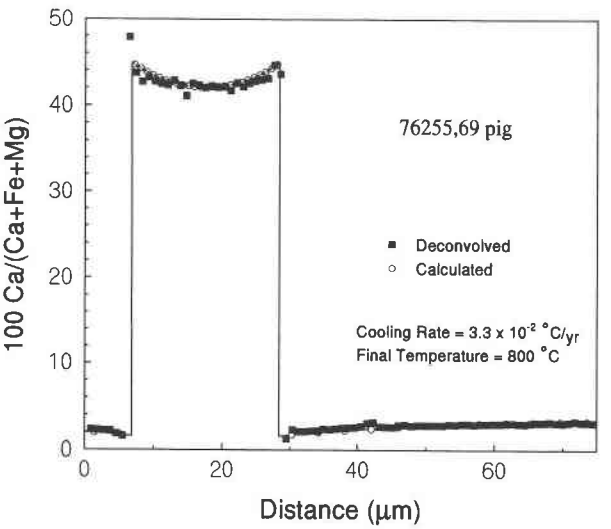

FIGURE 8. Measured (deconvolved) and calculated profiles in a traverse across pigeonite host and augite lamella from gabbronorite 76255,69. Value of ϵ is 0.55. Note that the lamellae in pigeonite are much wider than those in the coexisting augite.

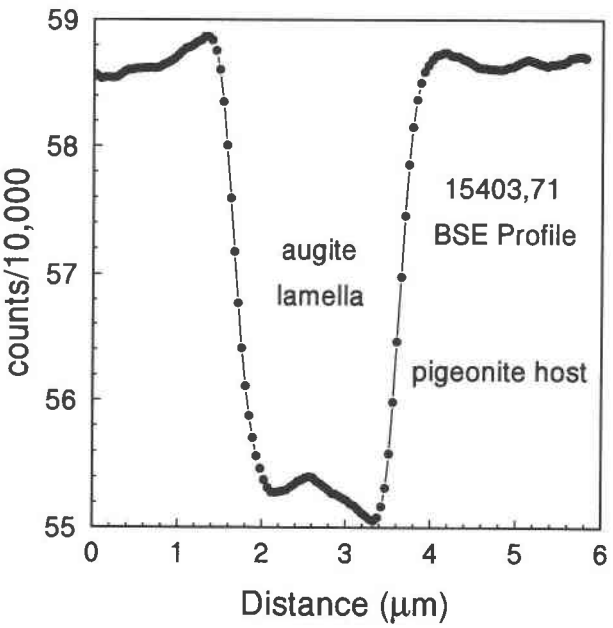

FIGURE 10. BSE profile for ferropigeonite from 15403,71.

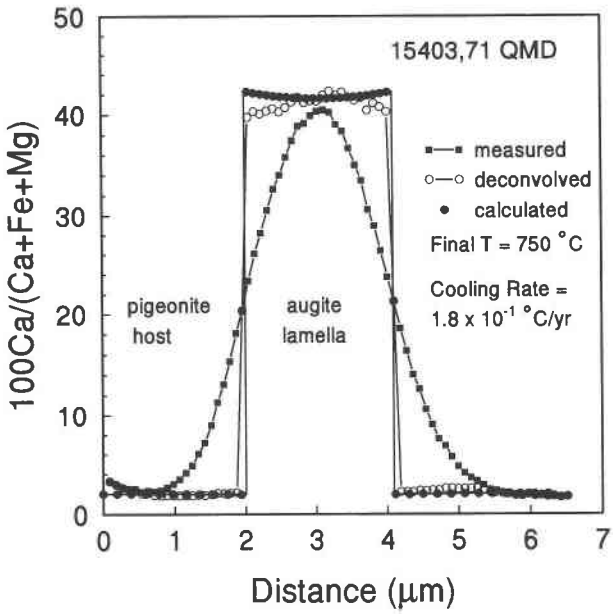

FIGURE 11. Measured pyroxene compositions, deconvolved compositions, and calculated profile for the same area of 15403,71 as shown in the BSE image in Figure 10. Value of ϵ is 0.55. Note that the BSE image shows much better resolution and the presence of small diffusion gradients at lamellar boundaries.

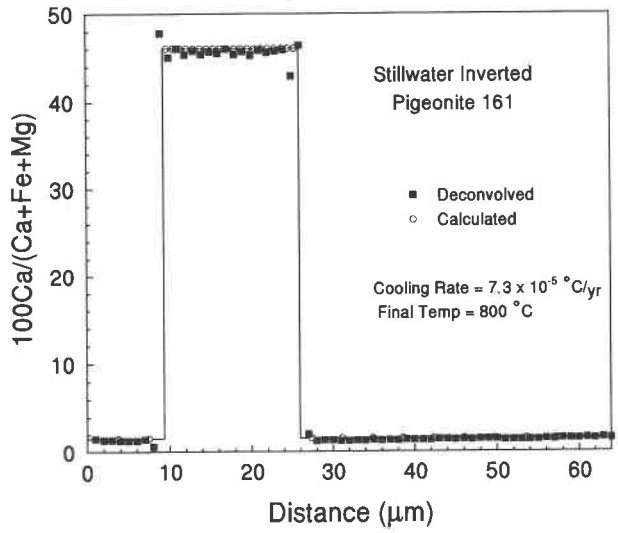

FIGURE 12. Measured (deconvolved) and calculated profiles in a traverse across inverted pigeonite host and augite lamella from Stillwater Complex gabbronorite 161. Value of ϵ is 0.55.

a finely exsolved ferropigeonite obtained by beam scanning over a 24 h period is shown in Figure 3f. The size of the excitation volume limits the resolution of this image; a Monte Carlo simulation of Ca$K\alpha$ X-ray production at 15 keV in diopside indicates that the excitation volume is nearly spherical and roughly 2 μm in diameter. A profile (Fig. 10) across the higher resolution BSE image (Fig. 3e) shows a W shape characteristic of diffusion profiles. Because the standard step-scanning method provides little useful data for narrow lamellae of this type, measured profiles were determined from the X-ray images. A Ca/(Ca + Mg + Fe) profile across the widest ferroaugite lamella is shown in Figure 11. To deconvolve this profile, correction factors for beam-overlap effects were calculated using the method of Ganguly et al. (1988) and 0.09 μm steps across a vertical pigeonite-augite interface. The correction factors were then applied to the measured profile to compute a deconvolved profile (Fig. 11). The necessity of deconvolution in the analysis of narrow lamellae is clearly demonstrated in this case. The best-fit calculated profile gives a cooling rate of 1.8×10^{-1} °C/yr for this sample (Fig. 11).

Stillwater Complex

Sample 161, a gabbronorite from GN-III near the top of the exposed section of the Stillwater Complex, contains inverted pigeonite with well-developed (001) exsolution lamellae of augite (Fig. 3d). The lamellae are commonly arranged in a herringbone pattern, indicating that they exsolved from a twinned monoclinic pigeonite prior to inversion. Major elements show no compositional gradients, whereas Al shows a slight gradient. The computed profile provides a good fit to the deconvolved profile (Fig. 12). The cooling rate of 7.3×10^{-5} is similar to those determined for the ferroan anorthosite samples.

DISCUSSION

Depth of burial

Inversion of a cooling rate to a unique depth of burial is not possible without additional information on the geometry and thermal state of the cooling body and its surroundings. To compound the problem, measured values of the thermal diffusivity vary widely, and the problem is particularly severe in the lunar case because of the presence of a thick regolith that existed early in lunar history. Materials in porous regoliths might be expected to have significantly lower thermal conductivities. Consequently, the estimation of burial depth is the least well-constrained aspect of the problem. Lacking the controls on geometry and thermal states that would justify a more rigorous approach, we chose to use the data from the Stillwater pyroxene to calibrate cooling rates as a function of depth because, in the case of Stillwater samples, geobarometry provides an independent measure of the depth of burial. Assemblages in the hornfels exposed at the base of the complex indicate equilibration at pressures between 3 and 4 kbar at 825 °C (Labotka 1985), which correspond to depths between 11 and 15 km. We assume a depth of 13 $\pm$ 2 km for the lower contact of the complex. We estimate that at the time of crystallization of the pigeonite in sample 161, which was used as our calibrating sample, the depth of cover was 11 $\pm$ 2 km. Lava flows, lava lakes, and sills (and presumably magma oceans) closely follow the relationship $Z = C \times \sqrt{t}$, where Z is the depth in meters to a particular isotherm, t is the cooling time in

TABLE 2. Cooling rates and depths of burial

	T_i (°C)	T_f (°C)	Cooling rate (°C/yr)	Depth (km)
67075,52 Aug	1087	800	3.7×10^{-5}	14
60025,130 Aug	1097	800	1.8×10^{-5}	21
76255,69 Aug	1117	800	3.2×10^{-2}	0.5
76255,69 Pig	1136	800	3.3×10^{-2}	0.5
67915,190 Pig	1070	825	3.7×10^{-2}	0.5
15403,71 Pig	1024	750	1.8×10^{-1}	0.2
SWC 161 Pig	1130	800	7.3×10^{-5}	11

years, and C is a constant dependent on the thermal diffusivity. The calculated cooling rate for Stillwater pigeonite of 7.3×10^{-5} °C/yr over the temperature range from 1130 to 800 °C gives a value of $C = 5.2 \pm 1.0$. An independent estimate of the value for C can be obtained from the magma-ocean thermal evolution models of Solomon and Longhi (1977). From the thermal model that they rate as their most complete, a value of $C = 4.4$ is obtained if Z represents the distance from the surface to the base of the crust, i.e., the magma-ocean solidus. Given the unknown factors discussed above and the uncertainties in thermal conductivities, more sophisticated thermal models are not warranted. Although the computations of absolute depths of burial could be in error by a significant amount, we feel that there is an internal consistency in the method described above and that the results have meaning in a relative sense. Results (on the basis of $C = 5.2$) are summarized in Table 2.

The most striking result of our study is the large difference in depth of burial between the ferroan anorthosite suite and the Mg-suite samples. If the upper crust is dominated by ferroan anorthosite, as is commonly assumed, then this crustal layer extends to depths of tens of kilometers. The highland magnesian and alkali suite samples examined in this study have much more rapid cooling rates and probably formed as cumulates in intrusions emplaced within the uppermost crust. This conclusion agrees with that of Ryder (1992), who presented mineralogic evidence indicating that Mg-suite dunite 72415 crystallized at a depth of <1 km. Troctolite sample 76535, a member of the Mg suite, may be a possible exception to this general conclusion. Gooley et al. (1974) suggested that this rock formed at a depth between 10 and 20 km. However, the original geobarometric calculations on 76535 were based on simple solution models now known to be incorrect.

Lunar crustal stratigraphy

Virtually all the large ferroan anorthosite samples in the collection are from the Descartes Formation of the Central Highlands (Apollo 16). The data presented in this paper indicate that ferroan anorthosite was excavated from depths of up to 20 km in this area. Because Descartes material was derived from the upper crustal levels at the impact site of the Nectaris basin (Spudis 1993), it is reasonable to conclude that ferroan anorthosite is the dominant upper crustal rock type in this region. However, the composition of the upper crust north and west of the Central Highlands is much more problematic. Ferroan anorthosite is rare in the Imbrium ejecta at the Apennine front (Apollo 15) and Fra Mauro region (Apollo 14) and absent from the Serenitatis region sampled by Apollo 17. Either the anorthositic upper layers of the lunar crust were removed from a significant fraction of the nearside by pre-Serenitatis impact events, or no ferroan anorthositic layers ever formed in this region.

In contrast, Mg-suite samples are common in the Imbrium, Serenitatis, and Fra Mauro areas, and cooling rates calculated for these samples are consistent with their formation as cumulates in high-level magma chambers emplaced into the upper crust during the first 600 m.y. of lunar history. The Fra Mauro Formation breccias (Apollo 14) provide the best indicator of the makeup of the pre-Imbrium upper crust in this region of the Moon. These breccias have an overall mafic composition and comprise a complex mixture of Mg-suite clasts, KREEP fragments, and older mare basalts. Magmatism in the form of lava flows and subjacent plutons was apparently active in Imbrium and Serenitatis regions of the Moon during pre-Imbrium times possibly in response to crustal thinning by impact processes and mantle rebound (Zuber et al. 1995).

Evidence on the constitution of the middle to lower crust is less direct because no crystalline samples in the sample collection can be unequivocally assigned to these crustal layers. Impact melts associated with the largest basins provide the best opportunity to deduce lower crustal stratigraphy. Low-K Fra Mauro (LKFM) "basalt" composition is a ubiquitous component of Apollo 15 and 17 soils and forms the matrix of melt-rich, fragment-laden breccias at these sites. These melts are believed to be representative of the main melt sheets now largely covered by mare basalts. Cratering models are consistent with the formation of LKFM by impact melting of middle and lower crust layers (Ryder and Wood 1977; Spudis 1993). Apollo 15 LKFM melts are more mafic, poorer in KREEP, and have higher Mg/(Mg + Fe) than the Apollo 17 LKFM melts. Because the Imbrium impact excavated material from a deeper level of the crust, it can be concluded that the middle to lower crust (30–50 km) becomes progressively more mafic and KREEP poor with depth. Appropriate protoliths of the LKFM melts, and by inference the main rock types in the middle to lower crust, are noritic and troctolitic cumulates formed during global magma-ocean differentiation.

The inferred decrease in the abundance of the KREEP component with depth in the middle and lower crust leads to the conclusion that a KREEP-rich layer is located at some intermediate layer within the crust rather than at the crust-mantle boundary. KREEP is widely believed to be a late-stage residue from fractionation of the magma ocean, and, as such, it is analogous to the Sandwich Horizon in the Skaergaard Intrusion, which is located above a thick sequence of gabbroic and troctolitic cumulates. There is no compelling reason to place the KREEP layer at the crust-mantle boundary as is commonly done.

One of the most interesting aspects of lunar science is the apparent absence among the returned lunar samples of crystalline rocks that can be unequivocally assigned to the upper mantle or lower crust. Samples that may have been derived from the lower crust occur in the form of LKFM impact melts. The closest crystalline equivalents of this composition are the Apollo 17 norite samples, which, however, have geochemical affinities, e.g., low Ti/Sm, low Sc/Sm, high REE, with other highland Mg-suite samples that formed by accumulation in high-level chambers. Norite formed during crystallization of the lunar magma ocean would have the trace element characteristics of the ferroan anorthosite, as is the case for cogenetic norite, troctolite, gabbronorite, and anorthosite formed during fractionation and accumulation of terrestrial layered intrusions. Because such norite is not present in the lunar collection, the possibility must be seriously considered that crystalline samples derived from the lower crust are absent, or very rare, on the lunar surface.

Acknowledgments

This work was supported by NASA grant NAGW-3352. We thank Kiyoshi Fujino for providing us with unpublished data on interdiffusion coefficients in pyroxene and Mark Ghiorso for permitting us to use a prepublication version of his pyroxene solvus. We thank Graham Ryder and Jibamitra Ganguly for perceptive and very useful reviews.

References cited

Brady, J.B., and McCallister, R.H. (1983) Diffusion data for clinopyroxenes from homogenization and self-diffusion experiments. American Mineralogist, 68, 95–105.

Carlson, R.W., and Lugmair, G.W. (1988) The age of ferroan anorthosite 60025: Oldest crust on a young moon. Earth and Planetary Science Letters, 90, 119–130.

Fujino, K., Nachara, H., and Momoi, H. (1990) Direct determination of cation diffusion coefficients in pyroxenes. Eos, 71, 943–944.

Ganguly, J., Bhattacharya, R.N., and Chakraborty, S. (1988) Convolution effect in the determination of compositional profiles and diffusion coefficients by microprobe step scans. American Mineralogist, 73, 901–909.

Ganguly, J., and Tazzoli, V. (1994) Fe^{2+}-Mg interdiffusion in orthopyroxene: Retrieval from the data on intracrystalline exchange reaction. American Mineralogist, 79, 930–937.

Gooley, R., Brett, R., Warner, J., and Smyth, J.R. (1974) A lunar rock of deep crustal origin: Sample 76535. Geochimica et Cosmochimica Acta, 38, 1329–1340.

Hawke, B.R., Peterson, C.A., Lucey, P.G., Taylor, G.J., Blewett, D.T., and Spudis, P.D. (1995) Remote sensing studies of lunar anorthosite deposits. Lunar and Planetary Science, XXVI, 563–564.

James, O.B. (1980) Rocks of the early lunar crust. Proceedings of the 11th Lunar and Planetary Science Conference, 365–393.

James, O.B., and Flohr, M.K. (1983) Subdivision of the Mg-suite noritic rocks into Mg-gabbronorites and Mg-norites. Proceedings of the 13th Lunar and Planetary Science Conference, Journal of Geophysical Research, 88, supplement, p. A603–A614.

James, O.B., Lindstrom, M.M., and McGee, J.J. (1991) Lunar ferroan anorthosite 60025: Petrology and chemistry of mafic lithologies. Proceedings of the Lunar and Planetary Science Conference, 21, 63–87.

Labotka, T.C. (1985) Petrogenesis of the metamorphic rocks beneath the Stillwater Complex: Assemblages and conditions of metamorphism. In G.K. Czamanske and M.L. Zientek, Eds., The Stillwater Complex, Montana: Geology and guide. Montana Bureau of Mines and Geology Special Publication, 92, 70–76.

Lindsley, D.H. (1983) Pyroxene thermometry. American Mineralogist, 68, 477–493.

Marvin, U.B., Lindstrom, M.M., Holmberg, B.B., and Martinez, R.R. (1991) New observations on the quartz monzodiorite-granite suite. Proceedings of the Lunar and Planetary Science Conference, 21, 119–135.

McCallum, I.S., Okamura, F.P., and Ghose, S. (1975) Mineralogy and petrology of sample 67075 and the origin of lunar anorthosites. Earth and Planetary Science Letters, 26, 36–53.

Miyamoto, M., and Takeda, H. (1994) Evidence for excavation of deep crustal material of a Vesta-like body from Ca compositional gradients in pyroxene. Earth and Planetary Science Letters, 122, 343–349.

Norman, M.D., and Ryder, G. (1980) Geochemical constraints on the igneous evolution of the lunar crust. Proceedings of the 11th Lunar and Planetary Science Conference, 317–331.

Nyquist, L.E., Reimold, W.U., Bogard, D.D., Wooden, J.L., Bansal, B.M., Weisman, H., and Shih, C.-Y. (1981) A comparative Rb-Sr, Sm-Nd and K-Ar study of shocked norite 78236: Evidence of slow cooling in the lunar crust? Proceedings of the Lunar and Planetary Science Conference, 12B, 67–97.

Premo, W.R., and Tatsumoto, M. (1992) U-Th-Pb, Rb-Sr, and Sm-Nd isotopic systematics of lunar troctolite cumulate 76535: Implications on the age and origin of this early deep-seated cumulate. Proceedings of the Lunar and Planetary Science Conference, 22, 381–397.

——(1993) U-Pb isotopic systematics of ferroan anorthosite 60025. Lunar Planetary Science, XXIV, 1173–1174.

Ryder, G. (1982) Lunar anorthosite 60025, the petrogenesis of lunar anorthosites, and the composition of the Moon. Geochimica et Cosmochimica Acta, 46, 1591–1601.

——(1992) Chemical variation and zoning of olivine in lunar dunite 72415: Near-surface accumulation. Proceedings of the Lunar and Planetary Science Conference, 22, 373–380.

Ryder, G., and Wood, J.A. (1977) Serenitatis and Imbrium impact melts: Implications for large-scale layering in the lunar crust. Proceedings of the 8th Lunar and Planetary Science Conference, 655–668.

Sack, R.O., and Ghiorso, M.S. (1994) Thermodynamics of multicomponent pyroxenes: II. Phase relations in the quadrilateral. Contributions to Mineralogy and Petrology, 116, 287–300.

Sanford, R.F. (1982) Three FORTRAN programs for finite-difference solutions to binary diffusion in one and two phases with composition- and time-dependent diffusion coefficients. Computers and Geosciences, 8, 235–263.

Shih, C.-Y., Nyquist, L.E., Dasch, E.J., Bogard, D.D., Bansal, B.M., and Weismann, H. (1993) Ages of pristine noritic clasts from lunar breccias 15445 and 15455. Geochimica et Cosmochimica Acta, 57, 915–931.

Simonds, C.H., Phinney, W.C., and Warner, J.L. (1974) Petrography and classification of Apollo 17 non-mare rocks with emphasis on samples from the Station 6 boulder. Proceedings of the 5th Lunar Science Conference, 337–353.

Solomon, S.C., and Longhi, J. (1977) Magma oceanography: 1. Thermal evolution. Proceedings of the 8th Lunar and Planetary Science Conference, 583–599.

Snyder, G.A., and Taylor, L.A. (1995) The growth and modification of lunar crust: KREEP basalt crystallization and precipitation of Mg- and alkali suite cumulates. Lunar Planetary Science, XXVI, 1325–1326.

Spudis, P.D. (1993) The geology of multi-ring impact basins, 263 p. Cambridge University Press, U.K.

Taylor, G.J., Warner, R., Keil, K., Geiss, J., Marti, K., Roedder, E., Schmitt, R.A., and Weiblin, P. (1979) The 67915 consortium: Searching for pieces of the ancient lunar crust. In Papers presented to the Conference on the Lunar Highland Crust, p. 169–171. Lunar and Planetary Institute, Houston, Texas.

Warren, P.H. (1990) Lunar anorthosites and the magma-ocean plagioclase-flotation hypothesis: Importance of FeO enrichment in the parent magma. American Mineralogist, 75, 46–58.

Zuber, M.T., Smith, D.E., Neumann, G.A., and Lemoine, F.G. (1995) Gravity, topography, and the geophysics of the Moon from the Clementine Mission. Lunar and Planetary Science, XXVI, 1581–1582.

Manuscript received July 17, 1995
Manuscript accepted May 17, 1996